

Fast 2D Bicephalous Convolutional Autoencoder for Compressing 3D Time Projection Chamber Data

Yi Huang
yhuang2@bnl.gov
Brookhaven National Lab
USA

Shinjae Yoo
sjyoo@bnl.gov
Brookhaven National Lab
USA

Yihui Ren
yren@bnl.gov
Brookhaven National Lab
USA

Jin Huang
jhuang@bnl.gov
Brookhaven National Lab
USA

ABSTRACT

High-energy large-scale particle colliders produce data at high speed in the order of 1 terabytes per second in nuclear physics and petabytes per second in high energy physics. Developing real-time data compression algorithms to reduce such data at high throughput to fit permanent storage has drawn increasing attention. Specifically, at the newly constructed sPHENIX experiment at the Relativistic Heavy Ion Collider (RHIC), a time projection chamber is used as the main tracking detector, which records particle trajectories in a volume of three-dimensional (3D) cylinder. The resulting data are usually very sparse with occupancy around 10.8%. Such sparsity presents a challenge to conventional learning-free lossy compression algorithms, such as SZ, ZFP, and MGARD. The 3D convolutional neural network (CNN)-based approach, *Bicephalous Convolutional Autoencoder* (BCAE), outperforms traditional methods both in compression rate and reconstruction accuracy. BCAE can also utilize the computation power of graphical processing units suitable for deployment in a modern heterogeneous high-performance computing environment. This work introduces two BCAE variants: BCAE++ and BCAE-2D. BCAE++ achieves a 15% better compression ratio and a 77% better reconstruction accuracy measured in mean absolute error compared with BCAE. BCAE-2D treats the radial direction as the channel dimension of an image, resulting in a 3× speedup in compression throughput. In addition, we demonstrate an unbalanced autoencoder with a larger decoder can improve reconstruction accuracy without significantly sacrificing throughput. Lastly, we observe both the BCAE++ and BCAE-2D can benefit more from using half-precision mode in throughput (76 – 79% increase) without loss in reconstruction accuracy. The source code and links to data and pretrained models can be found at https://github.com/BNL-DAQ-LDRD/NeuralCompression_v2.

CCS CONCEPTS

• **Applied computing** → **Physical sciences and engineering: Physics**;

Permission to make digital or hard copies of part or all of this work for personal or classroom use is granted without fee provided that copies are not made or distributed for profit or commercial advantage and that copies bear this notice and the full citation on the first page. Copyrights for third-party components of this work must be honored. For all other uses, contact the owner/author(s).

SC-W 2023, November 12–17, 2023, Denver, CO, USA

© 2023 Copyright held by the owner/author(s).

ACM ISBN 979-8-4007-0785-8/23/11.

<https://doi.org/10.1145/3624062.3625127>

KEYWORDS

deep learning, autoencoder, high-throughput inference, data compression, sparse data, high energy and nuclear physics

ACM Reference Format:

Yi Huang, Yihui Ren, Shinjae Yoo, and Jin Huang. 2023. Fast 2D Bicephalous Convolutional Autoencoder for Compressing 3D Time Projection Chamber Data. In *Workshops of The International Conference on High Performance Computing, Network, Storage, and Analysis (SC-W 2023)*, November 12–17, 2023, Denver, CO, USA. ACM, New York, NY, USA, 8 pages. <https://doi.org/10.1145/3624062.3625127>

1 INTRODUCTION

High-energy particle accelerators, such as the Large Hadron Collider (LHC) [7] and the Relativistic Heavy Ion Collider (RHIC) [17], play a critical role in advancing knowledge about the fundamental building blocks of the universe. Particle accelerators work by accelerating charged particles close to the speed of light and colliding them, where they interact and produce new subatomic particles. Particle detectors are built around the collision point to detect these particle products, which encode the information about interactions at the collision. Basically, a tracking detector acts as a camera capturing three-dimensional (3D) particle trajectories. If there is a particle passing through it, each pixel or voxel will register an analog-to-digital (ADC) number above a zero-suppression threshold. This 3D “camera” can work with a large number of channels (millions to billions) at a high frame rate (10 kHz to GHz), producing a large amount of ADC data.

Specifically, the recently constructed sPHENIX experiment at RHIC [17] consists of layers of tracking and calorimeter detectors aiming to study the microscopic nature of strongly interacting matter, ranging from nucleons to the strongly coupled quark-gluon plasma. Most sPHENIX data come from its main tracking detector, a Time Projection Chamber (TPC) (shown in Figure 1). sPHENIX TPC digitizes 42M-voxels 3D pictures of the collision continuously at 77 kHz. Traditionally, to reduce and store the data in time, a filtering system, called *level-1 trigger*, has been used. The trigger determines which data are more valuable, leading to a small subset of data being selected and stored for later analysis. Instead of a level-1 trigger, developing a high-throughput real-time compression algorithm to reduce and store *all* collision signals has become increasingly important for future collider experiments with streaming data acquisition (DAQ) that aims to record all collisions [1, 5].

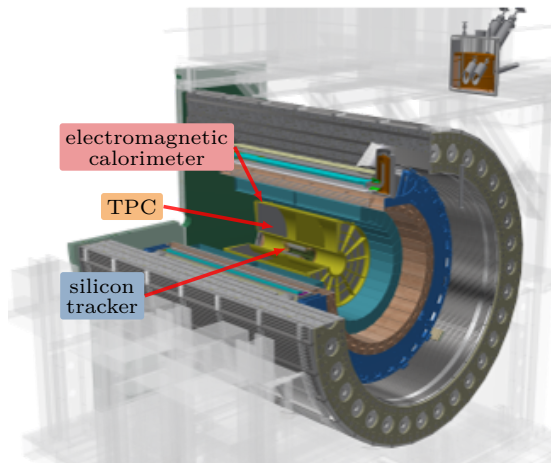


Figure 1: Detector model.

There is abundant literature in the lossy compression community, but few existing methods have been optimized or designed for sparse 3D TPC data. For example, the effectiveness of the error-bounded SZ [6, 14, 18] compression algorithm method has been demonstrated in climate science and cosmology data. The fixed-rate compression method (ZFP) [13] has been motivated by hydrodynamics simulations, while the MultiGrid Adaptive Reduction of Data (MGARD) [2, 11] method has been developed for compressing turbulent channel flow and climate simulation. We hypothesize that most data challenges impacting the high-performance computing (HPC) community stem from distributed high-fidelity simulation in climate science, fluid dynamics, cosmology, and molecular dynamics. Therefore, by introducing this unique challenge from the particle accelerator community, we seek to ignite research interest in the scientific data reduction community. Although all these compression algorithms have demonstrated reasonable performance with 3D TPC data, a specially designed neural network-based model, *Bicepheulous Convolutional Auto-Encoder* (BCAE) [10], can outperform them in both compression rate and reconstruction accuracy. However, as an initial proof-of-concept, BCAE has some drawbacks, including suboptimal compression throughput.

This work proposes an improved version of BCAE, called *BCAE++*, which improves the compression ratio from 27 to 31 and decreases the mean absolute error (MAE) from .198 to .112. MAE is an indicator of reconstruction accuracy—the lower, the better. We also introduce a two-dimensional (2D) variant of BCAE, *BCAE-2D*, by replacing 3D CNN layers with a 2D one and treating the radial dimension of the TPC data as a channel dimension. This change has resulted in 3× speedup in throughput. Because only the encoder portion of the auto-encoder neural network architecture will be used in real time and the decoder (decompression) can be used offline, this work also explores if expanding the number of decoder parameters can improve reconstruction accuracy. Lastly, we demonstrate a post-training “trick” using the half-precision representation of a network. It can enhance the throughput by over 70% without losing reconstruction accuracy.

2 TPC DATA AND BCAE COMPRESSION METHODS

2.1 TPC Data Preparation

Figure 1 shows that the sPHENIX TPC is a perfect testbed for developing a high-throughput real-time compression algorithm. It is located between the inner silicon vertex tracker and the electromagnetic calorimeter. Along the radial dimension, the TPC is composed of 48 cylindrical layers of small sensors, which are grouped into three layer groups: inner, middle, and outer. Each layer group has 16 consecutive layers. In the digitized data and for each TPC layer, the voxels are presented as a rectangular grid with rows along the z (or horizontal) direction and columns along the azimuthal direction. Within one layer group, all layers have the same number of rows and columns. This allows us to represent the ADC values from one layer group as a 3D array. This study focuses on the outer layer group, where the array of ADC values has shape (16, 2304, 498) in the radial, azimuthal, and horizontal orders.

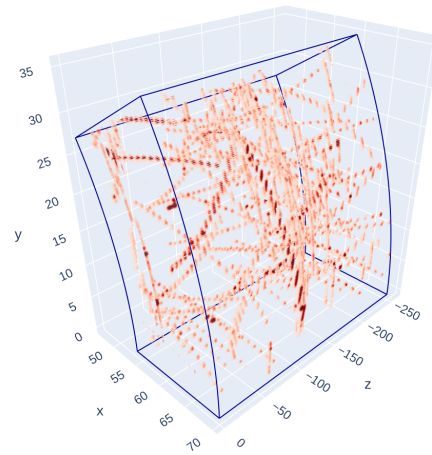


Figure 2: Example of a TPC Wedge. The z axis is in the horizontal direction. The x and y axes are on the plane spanned by the radial and azimuthal directions.

To match the subdivision of the TPC data assembly module in the readout chain, the voxel data are divided into 24 equal-size non-overlapping sections: 12 along the azimuthal direction (30 degrees per section) and 2 along the horizontal direction (divided by the transverse plane passing the collision point). We call one such section a *TPC wedge* (Figure 2). The array of ADC values from each TPC wedge in the outer layer has shape (16, 192, 249), listed in radial, azimuthal, and horizontal directions, respectively. All ADC data from the same wedge will be transmitted to the same group of front-end electronics, after which a real-time lossy compression algorithm could be deployed. Therefore, TPC wedges are used as the direct input to the deep neural network compression algorithms.

Here, we use the simulation data of 1310 events for central $\sqrt{s_{NN}} = 200$ GeV Au+Au collisions with 170 kHz pile-up collisions. The data were generated with the HIJING event generator [20] and Geant4 Monte Carlo detector simulation package [4] integrated with the sPHENIX software framework [16]. The simulated TPC

readout (ADC values) from these events are represented in a 10-bit unsigned integer $\in [0, 1023]$. To reduce unnecessary data transmission between detector pixels and front-end electronics, a zero-suppression algorithm has been applied. All ADC values below 64 are suppressed to zero as most of them are noise. This zero-compression makes the TPC data sparse at about 10% occupancy (non-zero values).

We divide the 1310 total events into 1048 events for training and 262 for testing. Each event contains 24 outer-layer wedges. Thus, the training partition contains 25152 TPC outer-layer wedges, while the testing portion has 6288 wedges. The compression algorithm aims to compress each wedge independently.

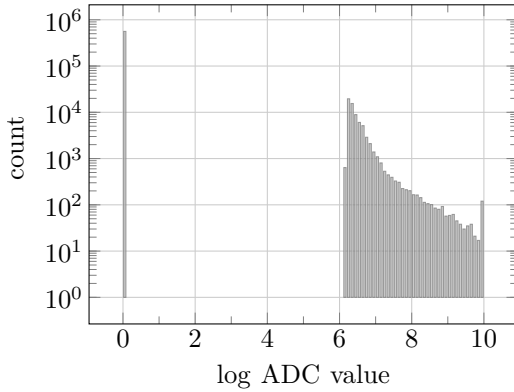


Figure 3: Log ADC distribution.

Finally, as trajectory locations must be interpolated from neighboring sensors using the ADC values, it is important to preserve the relative ADC ratio between the sensors. Hence, for this study, we trained autoencoders to reconstruct the *log ADC values* ($\log_2(\text{ADC}+1)$) instead of the raw ADC values. A log ADC value is a float number in $[0., 10.]$. Because of the zero-suppression at 64, all nonzero log ADC values exceed 6. The ground truth distribution of log ADC values is plotted in Figure 3.

2.2 Bicephalous Convolutional Auto-Encoder (BCAE)

An autoencoder [9] is composed of one encoder and one decoder. The output from the encoder is called a *code*. Autoencoders are commonly used for data compression. The compression ratio is defined as the ratio between the size of an input and its code—the smaller the code, the higher the compression ratio. The decoder takes in a code and produces a reconstruction of the input. The distance between the original input and the reconstruction is used as the loss function to train the autoencoder network. Although this approach may work well enough in cases where the input distribution is more regular (resembling a Gaussian distribution), it may struggle with a distribution such as those of zero-suppressed log ADC values [3, 8].

As evident in Figure 3, the log ADC value is bi-modal and has a sharp edge at 6.0. For this irregular distribution, we need renovated autoencoder structures. The BCAE [10] was proposed as a potential solution. As illustrated in Figure 4, in addition to the reconstruction

decoder D_{reg} , BCAE also has a segmentation decoder D_{seg} for voxel-wise bi-class classification. The segmentation decoder determines whether a voxel is zero (class 0) or nonzero (class 1). The output produced by D_{seg} is assessed using the focal loss \mathcal{L}_{seg} , a specialized loss function designed to address imbalanced datasets [12]. The output generated by the regression decoder D_{reg} is combined with that from D_{seg} to form the reconstruction of the input, which then is evaluated using a regression loss \mathcal{L}_{reg} . This study uses MAE for the regression loss.

Specifically, if we denote the total number of voxels by M and let \hat{l}_x be the output of D_{seg} for voxel x , the *focal loss* is defined to be

$$\mathcal{L}_{\text{seg}}(\{\hat{l}_x|x\}; \gamma) = \frac{1}{M} \sum_x -l_x \log_2(\hat{l}_x) (1 - \hat{l}_x)^\gamma - (1 - l_x) \log_2(1 - \hat{l}_x) (\hat{l}_x)^\gamma. \quad (1)$$

Here, $l_x = 1$ if the voxel is positive and 0 otherwise, and γ is the focusing parameter. We employ the focal loss because, on average, only 10.8% of ADC values are nonzero. In this study, we set the focusing parameter γ to be 2. Given a classification threshold h and let \hat{v}_x be the prediction for voxel x produced by D_{reg} , the masked prediction \tilde{v}_x is defined as $\tilde{v}_x = \hat{v}_x \mathbf{1}_{\hat{l}_x > h}$, where $\mathbf{1}$ is the characteristic function. Hence, the regression loss \mathcal{L}_{reg} is defined as

$$\mathcal{L}_{\text{reg}}(\{\tilde{v}_x, v_x|x\}; h) = \frac{1}{M} \sum_x |\tilde{v}_x - v_x|. \quad (2)$$

Finally, to manage the gap between 0 and 6, we adopt another technique proposed by [10] called *regression output transformation*. We apply an output activation function $T(x) = 6. + 3. \exp(x)$ to the output from the regression decoder. Note that by applying T , all regression output values are above 6., and the zero values in the reconstruction will result from the masking by segmentation output (refer to the definition of \tilde{v}_x).

2.3 BCAE++ and BCAE-HT

Two modifications are made to the original BCAE [10]. First, we pad the horizontal direction from length 249 to length 256 with zero. This makes halving the dimension more straightforward and enables using convolution/deconvolution with kernel size 4, padding 1, and stride 2 uniformly throughout the encoder and decoder construction. This change streamlines the neural network architecture search in a programmatic way. In addition, this modification reduces the code dimension from (8, 17, 13, 16) to (8, 16, 12, 16) and improves the BCAE compression ratio from 27.041 to 31.125. Zero-padding in the horizontal direction is clipped during the evaluation, so reconstruction accuracy metrics are not inflated. Second, we remove all the normalization layers in BCAE as they do not affect reconstruction performance significantly in a sufficiently long training. However, we can speed up training and inference without them. Based on these modifications, we constructed BCAE++ with a similar number of parameters to the original BCAE but with better performance (Table 1) and a larger compression ratio.

We also introduce a high-throughput (HT) variation, *BCAE-HT*. The difference between BCAE++ and BCAE-HT is in the number of features (output channels) in the four residual blocks of their respective encoders. For BCAE++, the numbers of features are

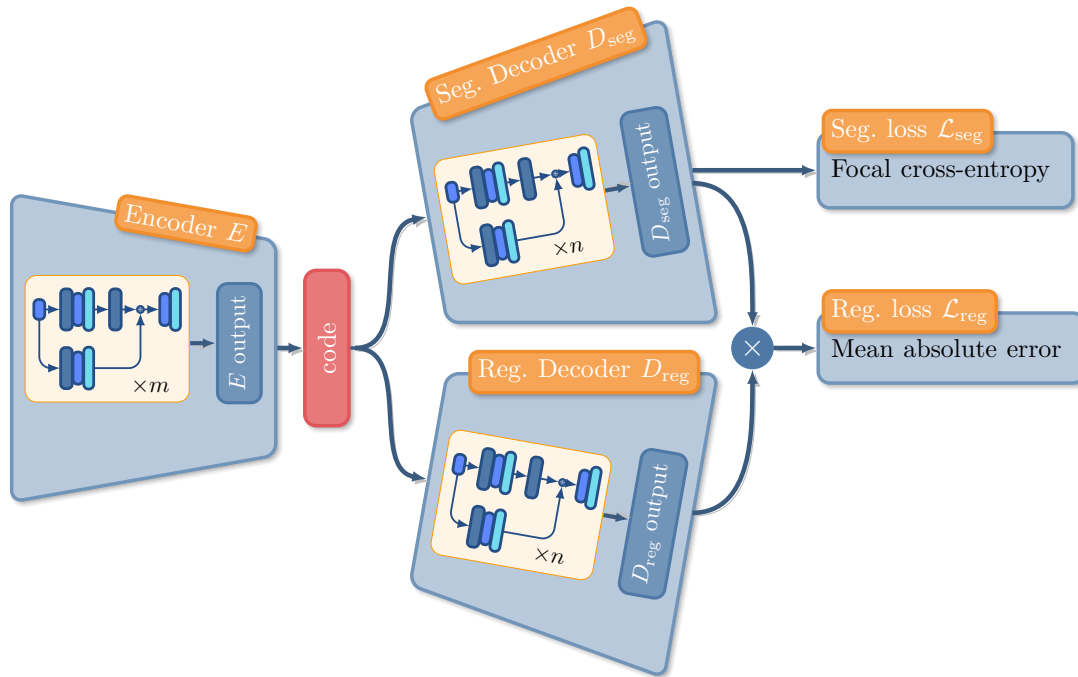


Figure 4: Bicephalous convolutional autoencoder (BCAE).

8, 16, 32, 32 (same as BCAE), while those for BCAE-HT are 2, 4, 4, 8. The change reduces the encoder size of BCAE-HT to 5% of those for BCAE and BCAE++ and yields a 76% improvement in throughput.

Algorithm 1: BCAE_encoder_2D

Input: number of blocks m , number of downsampling layers d
Output: A PyTorch module

- 1 Initialize network N to be an empty module list;
- 2 Append N with $L_{\text{in}} = \text{Conv2D}(i = 16, o = 32, k = 7, p = 3)$
- 3 **for** $i \leftarrow 1$ **to** m **do**
- 4 **if** $i \leq d$ **then**
- 5 Append N with $\text{AvgPool2D}(k = 2, s = 2)$;
- 6 Append N with two residual block
 $\text{Res}(i = 32, o = 32, k = 3, p = 1)$;
- 7 Append N with $L_{\text{out}} = \text{Conv2D}(i = 32, o = 16, k = 1)$;
- 8 **return** N ;

2.4 BCAE-2D

Due to the thinness of the TPC wedge along the radial dimension—16 layers versus 192 in the azimuthal and 249 in the horizontal dimensions—it may be more reasonable to treat the layer dimension as channels of an “image.” Moreover, while the layers all have different radii, the number of columns (along the azimuthal direction) in one layer group remains the same. This means the distance between two adjacent voxels along the azimuthal direction is farther apart in an outer layer than an inner one. This breaks the inductive

bias of translation invariance of a 3D convolution along the radial direction, making 2D convolution an even more appropriate choice for a TPC wedge.

We detail the construction of the 2D encoder and decoder in Algorithm 1 and Algorithm 2, respectively. The algorithms use i and o to denote the number of input and output channels, k to show kernel size, p to indicate padding (default is 0), and s to signify stride (default is 1).

Algorithm 2: BCAE_decoder_2D

Input: number of blocks n , number of upsampling layers d , output activation function A
Output: A PyTorch module

1 # NOTE: a decoder must have the same number of upsampling steps as the downsampling steps in its corresponding encoder

- 2 Initialize network N to be an empty module list;
- 3 **for** $i \leftarrow 1$ **to** n **do**
- 4 **if** $i \leq d$ **then**
- 5 Append N with $\text{Upsample}(\text{scale_factor} = 2)$;
- 6 Append N with two residual block
 $\text{Res}(i = 32, o = 32, k = 3, p = 1)$;
- 7 Append N with $L_{\text{out}} = \text{Conv2D}(i = 32, o = 16, k = 1)$;
- 8 Append N with output activation function A ;
- 9 **return** N ;

A BCAE-2D encoder E is constructed using `BCAE_encoder_2D` with two parameters: the number of encoder blocks m and number of downsampling layers d . The segmentation decoder D_{seg} is

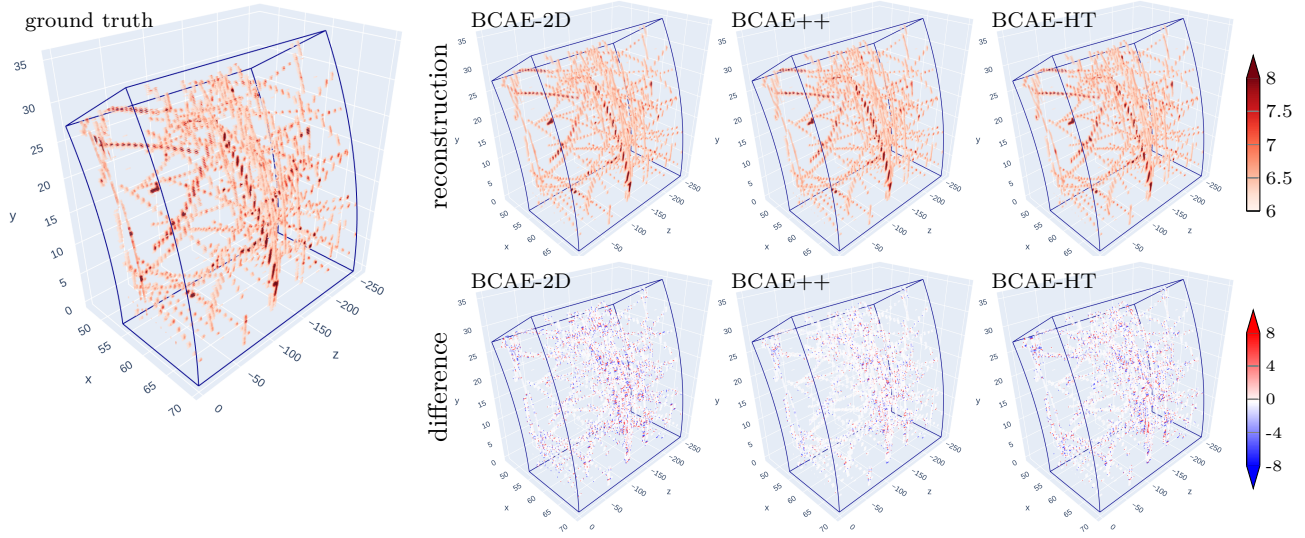


Figure 5: Reconstruction performance comparison.

constructed by `BCAE_decoder_2D` with `Sigmoid` as the output activation function A , while the regression decoder D_{reg} is constructed with the identity function as A . The number of upsampling layers d in the decoders must be equal to the number of downsampling layers in their corresponding encoder. For simplicity in this study, we construct the two decoders in a BCAE-2D model with the same number of blocks (n). Hence, a BCAE-2D model can be denoted by $\text{BCAE-2D}(m, n, d)$, where m is the number of encoder blocks in Algorithm 1, n is the number of decoder blocks in Algorithm 2, and d is the number of downsampling/upsampling layers.

We keep d at 3 so the compression ratio of a BCAE-2D model is the same as the 3D variants. A BCAE-2D model with $d = 3$ produces code with shape $(32, 24, 32)$. In Section 3.5, we conduct a grid search on the numbers of encoder and decoder blocks. After balancing reconstruction accuracy and throughput, we choose $\text{BCAE-2D}(m = 4, n = 8, d = 3)$ to represent the BCAE-2D models. Hence, in the sequel, we use $\text{BCAE-2D}(m = 4, n = 8, d = 3)$ as the default BCAE-2D.

2.5 Training Procedure

We implement all BCAEs with PyTorch 2.0. The training is conducted on the 25152 outer-layer TPC wedges in the training partition of the datasets, while 6288 TPC wedges are reserved for testing. We set the classification threshold h in Equation (2) to be .5 for both training and testing. All BCAE models are trained with a batch size of 4, and we train all BCAE++ and BCAE-HT for 1000 epochs. The initial learning rate is set at 10^{-3} and remains constant for the first 100 epochs. In the remaining epochs, we decrease the learning rate by 5% every 20 epochs. All BCAE-2D models are trained for 500 epochs. We set the initial learning rate at 10^{-3} and keep it constant for the first 50 epochs. In the remaining epochs, we decrease the learning rate by 5% every 10 epochs. For all BCAE models, we use the AdamW [15] optimizer with $(\beta_1, \beta_2) = (0.9, 0.999)$ and weight decay 0.01.

To improve the classification performance, we balance the contribution of the segmentation and regression loss dynamically as follows: assume the segmentation and regression losses at epoch t are ρ_s^t and ρ_r^t , respectively. Denote the coefficient of the segmentation loss at epoch t by c_t . Then, the coefficient for \mathcal{L}_{seg} for epoch $t + 1$ is given by

$$c_{t+1} = \frac{.5c_t + (\rho_r^t / \rho_s^t)}{1.5}.$$

We set c_0 to be 2000.

3 RESULT

3.1 Compression Ratio

The compression ratio is computed by the ratio between the input and the code. Both input and code are treated as 16-bit float. As mentioned in Section 2.3 and 2.4, the shape of the code produced by the BCAE-2D is $(32, 24, 32)$, and those for BCAE++ and BCAE-HT are both $(8, 16, 12, 16)$. Because the TPC wedge has shape $(192, 249, 16)$, the compression ratio is 31.125 for all newly introduced BCAE variants. This is greater than the compression ratio of 27.041 in the original BCAE [10].

3.2 Comparing Encoder Model Size and Throughput

The encoder model size is measured in the number of trainable parameters. Encoder throughput is measured in the number of TPC wedges processed per second. The input and output are allocated in GPU memory. Therefore, the file system input/output (IO) and host-to-device data transfer are not considered. All throughput experiments are conducted on a single NVIDIA RTX A6000 GPU with driver version 535. On the software side, we used PyTorch 2.0 compiled with CUDA 12.2.

As shown in Table 1, BCAE++ has the largest encoder size of 226k parameters, followed by the original BCAE with 202k. The

Table 1: Performance, encoder model size, and throughput comparison. The encoder size is measured in the number of trainable parameters. The reconstruction accuracy metrics and throughput are all measured with half-precision mode. The best performance with respect to each metric is underlined.

model	MAE ↓	PSNR ↑	precision ↑	recall ↑	encoder size ↓	throughput ↑
BCAE-2D	0.152	11.726	0.906	0.907	169.0k	<u>~ 6.9k</u>
BCAE++	<u>0.112</u>	<u>14.325</u>	<u>0.934</u>	<u>0.936</u>	226.2k	~ 2.6k
BCAE-HT	0.138	12.376	0.916	0.915	<u>9.8k</u>	~ 4.6k
BCAE[10]	0.198	9.923	0.878	0.861	201.7k	~ 2.4k

BCAE-2D has 169k but significantly higher throughput. Reducing the number of BC AE++ parameters results in the BC AE-HT model size of 9.8k. Although better than BC AE++ (2.6k), the BC AE-HT’s throughput (4.6k) is not as high as BC AE-2D (6.9k).

3.3 Reconstruction Accuracy Comparison

We evaluated performance of the BC AEs using four metrics: MAE, peak signal-to-noise ratio (PSNR), precision, and recall. Here, precision and recall are defined as follows:

$$\text{precision} = \frac{\sum_x \mathbf{1}_{\hat{i}_x > h} \mathbf{1}_{x > 6}}{\sum_x \mathbf{1}_{\hat{i}_x > h}}; \quad \text{recall} = \frac{\sum_x \mathbf{1}_{\hat{i}_x > h} \mathbf{1}_{x > 6}}{\sum_x \mathbf{1}_{x > 6}}.$$

We compare BC AE-2D and BC AE++ performance in two computation modes shown in Table 2. Given that compressing in half-precision yields negligible performance degradation while significantly boosting throughput, it is the most likely computation model for future deployment. Hence, all BC AEs performance reported in Table 1 are obtained with the half-precision computation mode. BC AE++ achieves the best scores in all reconstruction measurements.

Figure 5 compares the reconstruction performance of BC AE-2D, BC AE++, and BC AE-HT on one test TPC wedge. The noticeably different plots (second row) indicate the reconstruction produced by BC AE++ is the most accurate.

3.4 Investigating Half-precision Speedup

Throughput is tested in two computation modes: full-precision and half-precision. In full-precision mode, the encoder weights and input are all set to 32-bit floats. In half-precision mode, we manually cast the encoder weights and input to 16-bit floats. In Figure 6A, for BC AE-2D and BC AE++, half-precision affords more than 70% improvement in throughput. In full-precision mode, BC AE-HT and BC AE-2D have a similar throughput of 4000 frames per second. However, BC AE-HT’s speedup is much less (Figure 6C). This is due to the extremely small model size (9.8k) of BC AE-HT after reducing the 3D convolution channel sizes from BC AE++’s (8, 16, 32, 32) to (2, 4, 4, 8). As shown in Figure 6D, Tensor Core units are not used by those time-consuming convolution computations.

3.5 Investigating Auto-encoder Design

Here, we study how the depth (the number of blocks) of a BC AE-2D model’s encoder and decoders influence its reconstruction accuracy. For this purpose, we conduct a grid search on the number of encoder blocks (m in Algorithm 1), ranging from 3 to 7, and

Table 2: Reconstruction accuracy in full- and half-precision computation mode.

model	mode	MAE	precision	recall
BCAE-2D	full	0.151937	0.905469	0.906916
	half	0.151965	0.905326	0.90705
BCAE++	full	0.112347	0.933817	0.935779
	half	0.112342	0.933852	0.935741
BCAE-HT	full	0.138443	0.915891	0.914562
	half	0.138441	0.915780	0.914701

number of decoder blocks (n in Algorithm 2), from 3 to 11. Figure 7 illustrates the reconstruction accuracy of BC AE-2D models in MAE, precision, and recall. While the performance benefits significantly from deepening the decoders, the influence of encoder depth is relatively ambiguous. The benefit of a deep encoder is more obvious only when it is paired with decoders that are significantly deeper. We also calculate the compression throughput in half-precision mode and demonstrate the result in Figure 6E. After balancing the reconstruction accuracy and compression throughput, we choose the BC AE-2D model with $m = 4$ encoder blocks and $n = 8$ decoder blocks to represent the BC AE-2D models.

4 CONCLUSION AND DISCUSSION

The TPC tracking detectors examined in this work represent a modern particle accelerator detector that produces a large volume of data at an extreme rate (1 TB/s to 1 PT/s). Unlike common simulation data from hydrodynamics, climate science, and cosmology, TPC data are zero-compressed and sparse, presenting a unique challenge to real-time data compression algorithms. We present two BC AE variants: BC AE++ and BC AE-2D. Compared to the BC AE, BC AE++ improves the compression rate by 15% and reconstruction accuracy by 77% measured in MAE. The BC AE-2D model treats the radial dimension of TPC data as a channel dimension and achieves a 3x speedup during inference compared to BC AE++.

Based on this initial effort, there are several research directions worthy of future pursuit. For example, to further optimize the neural network throughput performance, we want to incorporate network pruning, quantization, and sparse CNN techniques. We also seek to extend our throughput comparison to include results of GPU-accelerated conventional lossy compression methods, such

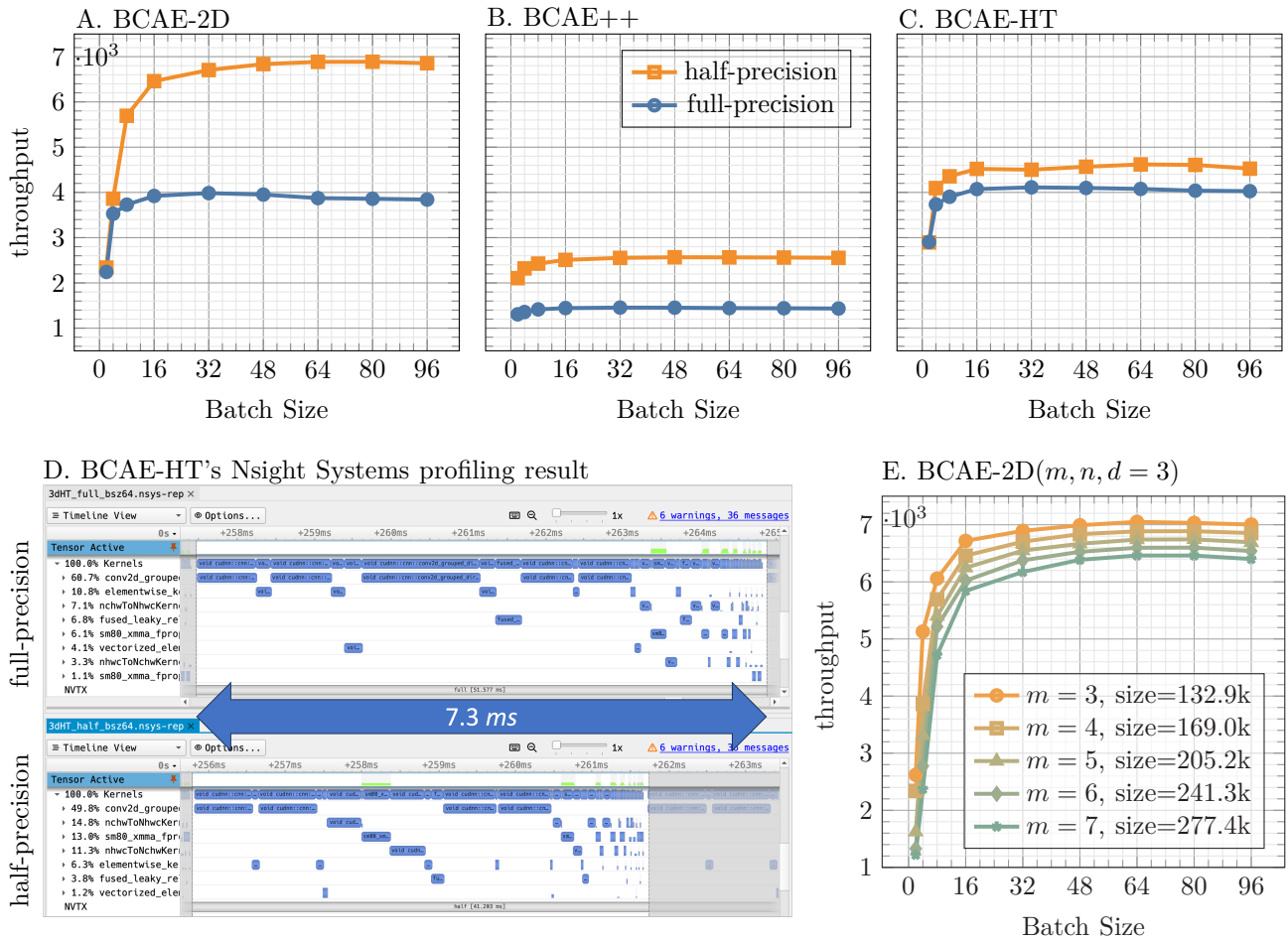


Figure 6: Panel A-C: Throughput in half- and full-precision modes on a single NVIDIA RTX A6000 GPU. Panel D: Diagnosing the lack of speedup by changing from full-precision to half-precision in the BC AE-HT model. This is due to small kernel sizes and the lack of Tensor Core activities. Panel E: Throughput in half-precision of BC AE-2D with $m = 3, 4, 5, 6, 7$ encoder blocks and 3 downsampling layers. The encoder size is measured in the number of parameters.

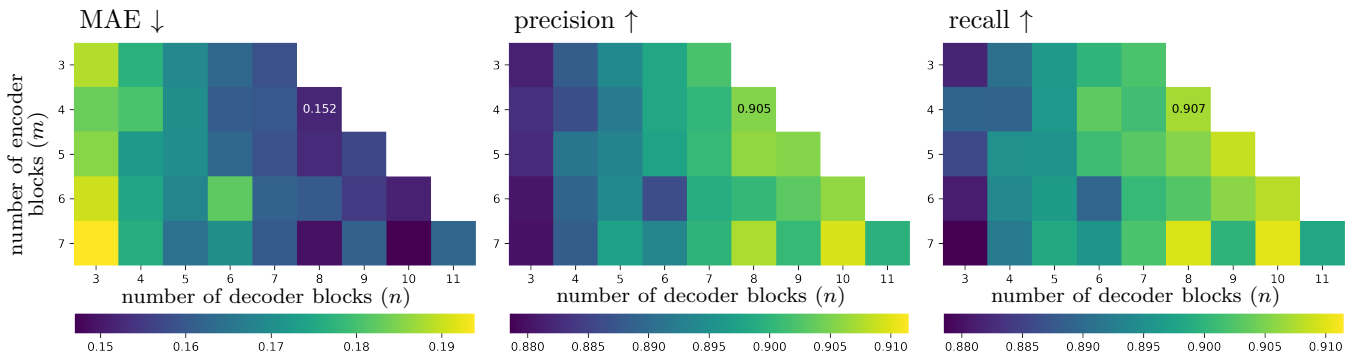


Figure 7: Reconstruction accuracy of BC AE-2D models with varying encoder and decoder depths.

as MGARD-GPU and cuSZ [19]. Finally, we anticipate this work

can attract additional research interest in particle detector data compression by the scientific data reduction community.

ACKNOWLEDGMENTS

This work was supported in part by Brookhaven National Laboratory under Laboratory Directed Research & Development No. 23-048 and the Office of Nuclear Physics within the U.S. DOE Office of Science under Contract No. DESC0012704.

REFERENCES

- [1] R. Abdul Khalek et al. 2022. Science Requirements and Detector Concepts for the Electron-Ion Collider: EIC Yellow Report. *Nucl. Phys. A* 1026 (2022), 122447. <https://doi.org/10.1016/j.nuclphysa.2022.122447> arXiv:2103.05419 [physics.ins-det]
- [2] Mark Ainsworth, Ozan Tugluk, Ben Whitney, and Scott Klasky. [n. d.]. Multilevel Techniques for Compression and Reduction of Scientific Data—The Multivariate Case. 41, 2 ([n. d.]), A1278–A1303. <https://doi.org/10.1137/18M1166651> Publisher: Society for Industrial and Applied Mathematics.
- [3] Yasir Alanazi, Nobuo Sato, Tianbo Liu, W. Melnitchouk, Michelle P. Kuchera, Evan Pritchard, Michael Robertson, Ryan Strauss, Luisa Velasco, and Yaohang Li. 2020. Simulation of electron-proton scattering events by a Feature-Augmented and Transformed Generative Adversarial Network (FAT-GAN). *arXiv preprint arXiv:2001.11103* (2020).
- [4] J. Allison et al. 2016. Recent developments in Geant4. *Nucl. Instrum. Meth. A* 835 (2016), 186–225. <https://doi.org/10.1016/j.nima.2016.06.125>
- [5] J. C. Bernauer et al. 2023. Scientific computing plan for the ECCE detector at the Electron Ion Collider. *Nucl. Instrum. Meth. A* 1047 (2023), 167859. <https://doi.org/10.1016/j.nima.2022.167859> arXiv:2205.08607 [physics.ins-det]
- [6] Sheng Di and Franck Cappello. [n. d.]. Fast Error-Bounded Lossy HPC Data Compression with SZ. In *2016 IEEE International Parallel and Distributed Processing Symposium (IPDPS)* (2016-05). 730–739. <https://doi.org/10.1109/IPDPS.2016.11> ISSN: 1530-2075.
- [7] Lyndon Evans and Philip Bryant. [n. d.]. LHC Machine. 3, 8 ([n. d.]), S08001. <https://doi.org/10.1088/1748-0221/3/08/S08001>
- [8] Bobak Hashemi, Nick Amin, Kaustuv Datta, Dominick Olivito, and Maurizio Pierini. 2019. LHC analysis-specific datasets with Generative Adversarial Networks. *arXiv e-prints* (2019), arXiv–1901.
- [9] G. E. Hinton and R. R. Salakhutdinov. [n. d.]. Reducing the Dimensionality of Data with Neural Networks. 313, 5786 ([n. d.]), 504–507. <https://doi.org/10.1126/science.1127647> Publisher: American Association for the Advancement of Science Section: Report.
- [10] Yi Huang, Yihui Ren, Shinjae Yoo, and Jin Huang. 2021. Efficient Data Compression for 3D Sparse TPC via Bicephalous Convolutional Autoencoder. In *2021 20th IEEE International Conference on Machine Learning and Applications (ICMLA)*. 1094–1099. <https://doi.org/10.1109/ICMLA52953.2021.00179>
- [11] Xin Liang, Ben Whitney, Jieyang Chen, Lipeng Wan, Qing Liu, Dingwen Tao, James Kress, David Pugmire, Matthew Wolf, Norbert Podhorszki, and Scott Klasky. [n. d.]. MGARD+: Optimizing Multilevel Methods for Error-Bounded Scientific Data Reduction. 71, 7 ([n. d.]), 1522–1536. <https://doi.org/10.1109/TC.2021.3092201> Conference Name: IEEE Transactions on Computers.
- [12] Tsung-Yi Lin, Priya Goyal, Ross Girshick, Kaiming He, and Piotr Dollár. 2017. Focal loss for dense object detection. In *Proceedings of the IEEE international conference on computer vision*. 2980–2988.
- [13] Peter Lindstrom. [n. d.]. Fixed-Rate Compressed Floating-Point Arrays. 20, 12 ([n. d.]), 2674–2683. <https://doi.org/10.1109/TVCG.2014.2346458> Conference Name: IEEE Transactions on Visualization and Computer Graphics.
- [14] Yuanjian Liu, Sheng Di, Kai Zhao, Sian Jin, Cheng Wang, Kyle Chard, Dingwen Tao, Ian Foster, and Franck Cappello. [n. d.]. Optimizing Error-Bounded Lossy Compression for Scientific Data With Diverse Constraints. 33, 12 ([n. d.]), 4440–4457. <https://doi.org/10.1109/TPDS.2022.3194695> Conference Name: IEEE Transactions on Parallel and Distributed Systems.
- [15] Ilya Loshchilov and Frank Hutter. 2017. Decoupled weight decay regularization. *arXiv preprint arXiv:1711.05101* (2017).
- [16] sPHENIX. 2019. sPHENIX Software repositories <https://github.com/sPHENIX-Collaboration>. (2019). <https://github.com/sPHENIX-Collaboration>
- [17] sPHENIX. 2019. Technical Design Report: sPHENIX experiment at RHIC. (2019). <https://indico.bnl.gov/event/5905/>
- [18] Dingwen Tao, Sheng Di, Zizhong Chen, and Franck Cappello. [n. d.]. Significantly Improving Lossy Compression for Scientific Data Sets Based on Multidimensional Prediction and Error-Controlled Quantization. In *2017 IEEE International Parallel and Distributed Processing Symposium (IPDPS)* (2017-05). 1129–1139. <https://doi.org/10.1109/IPDPS.2017.115> ISSN: 1530-2075.
- [19] Jiannan Tian, Sheng Di, Kai Zhao, Cody Rivera, Megan Hickman Fulp, Robert Underwood, Sian Jin, Xin Liang, Jon Calhoun, Dingwen Tao, and Franck Cappello. [n. d.]. cuSZ: An Efficient GPU-Based Error-Bounded Lossy Compression Framework for Scientific Data. In *Proceedings of the ACM International Conference on Parallel Architectures and Compilation Techniques* (New York, NY, USA, 2020-09-30) (PACT '20). Association for Computing Machinery, 3–15. <https://doi.org/10.1145/3410463.3414624>
- [20] Xin-Nian Wang and Miklos Gyulassy. 1991. HIJING: A Monte Carlo model for multiple jet production in p p, p A and A A collisions. *Phys. Rev. D* 44 (1991), 3501–3516. <https://doi.org/10.1103/PhysRevD.44.3501>